

Fission experiments with secondary beams

J BENLLIURE^a, S STEINHÄUSER^b, C BÖCKSTIEGEL^b, A GREWE^b, H-G CLERC^b,
A HEINZ^a, M DE JONG^b, A R JUNGHANS^a, J MÜLLER^b, K-H SCHMIDT^a and
M PFÜTZNER^c

^aGesellschaft für Schwerionenforschung m. b. H., Planckstrasse 1, 64291 Darmstadt, Germany

^bInstitut für Kernphysik, Technische Universität Darmstadt, Schlossgartenstrasse 9, 64289 Darmstadt, Germany

^cInstitute of Experimental Physics, University of Warsaw, Ul Hoza 69, 00-381 Warszawa, Poland

Abstract. Nuclear fission from excitation energies around 11 MeV was studied at GSI, Darmstadt for 76 neutron-deficient actinides and pre-actinides by use of relativistic secondary beams. The characteristics of multimodal fission of nuclei around ²²⁶Th are systematically investigated and related to the influence of shell effects on the potential-energy and on the level density between saddle point and scission. A systematic view on the large number of elemental yields measured gave rise to a new interpretation of the enhanced production of even elements in nuclear fission and allowed for a new understanding of pair breaking in fission.

Keywords. Nuclear reactions; radioactive beams; nuclear fission; shell effects.

PACS Nos 24.75+i; 25.85.-w; 25.85.Jg; 27.90.+b

1. Introduction

Nuclear fission provides unique information on the reordering of nucleons in a large-scale collective motion. The signatures of shell structure and pairing correlations show up in fission from low excitation energies. They have general implications on the influence of shell structure on nuclear dynamics and on the viscosity of cold nuclear matter. The use of secondary beams gives access to a large new field of fissioning systems by overcoming restrictions of conventional experimental techniques. In this contribution, the large body of data acquired in a recent experiment is presented and the resulting progress in the understanding of the fission dynamics is sketched.

2. Experiment

The secondary-beam facility of GSI, Darmstadt offers unique possibilities to provide secondary beams of neutron-deficient actinides and pre-actinides produced by fragmentation of relativistic ²³⁸U projectiles. Within the limits given by the primary-beam intensity and

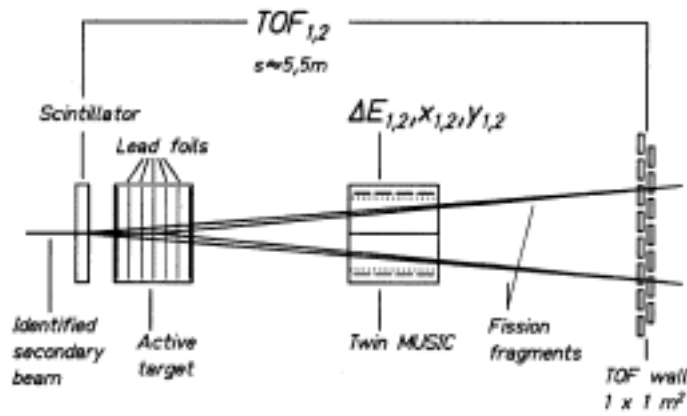


Figure 1. Schematical drawing of the set up for the fission experiment mounted behind the fragment separator.

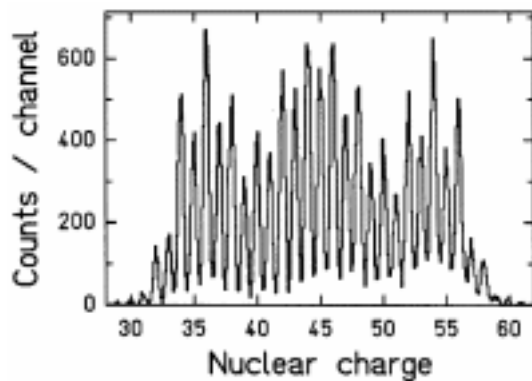


Figure 2. Nuclear-charge response of the twin MUSIC with velocity correction applied as obtained for the fission fragments after electromagnetic excitation of ^{226}Th projectiles.

the fragmentation cross sections [1,2], nuclear charge and mass number of the secondary projectiles can freely be selected by tuning the fragment separator [3].

Fission from the desired excitation-energy range slightly above the fission barrier was induced by electromagnetic interactions in a heavy target material. In the next section we give a detailed description of this excitation mechanism.

The experimental setup behind the fragment separator is sketched in figure 1. As secondary target we used a stack of lead foils with a total thickness of 3 g/cm^2 mounted in a gas-filled chamber which acts as a subdivided ionization chamber (active target). With this device it is possible to discriminate fission induced in the lead foils against fission induced in other layers, e.g. the scintillator. The average energy of the secondary projectiles in the lead target was about 430 A MeV. The differential energy loss of each fission fragment was measured separately with a horizontally subdivided twin ionization chamber. In order to correct the energy loss for the velocity dependence, the time-of-flight of

the fission fragments was measured by means of a (1m × 1m) scintillator wall. Figure 2 shows the nuclear-charge response of the experimental set up for fission fragments after electromagnetic-induced fission of ^{226}Th . Due to the high center-of-mass energies, an excellent charge resolution is achieved. Events stemming from reactions at lower impact parameters were suppressed. For details of the analysis procedure see refs [4,5].

3. Excitation mechanism

The electromagnetic excitation in-flight in the secondary target is one of the most important ingredients of the experiment, ideally adapted to the kinematic properties and to the low intensities of the secondary beams. It populates states in the vicinity of the fission barrier with large cross section of a few barns. Although the excitation energy acquired is not precisely known for a single event, the excitation-energy distribution can be calculated with rather good precision. The electromagnetic field of a lead target nucleus, seen by the projectile, can be represented by a flux of equivalent photons of different energies and multiplicities according to ref. [6]. The projectiles are excited according to the energy-dependent photo absorption cross section which is dominated by the giant dipole resonance with small contributions of the giant quadrupole resonances. First-chance fission represents the main source of fission, but also fission after evaporation of one or two particles (mostly neutrons) occurs with a probability of about 20%. This leads to a reduction of the excitation energy at fission. The excitation-energy distribution at fission after electromagnetic excitation of ^{234}U in the passage of a lead target at 430 A MeV is shown in figure 3 (for details of the calculation see ref. [4]). The calculated excitation-energy distributions of the other nuclei investigated are similar.

4. Results and discussion

In the present experiment, the elemental yields and the total kinetic energies of long isotopic chains from ^{205}At to ^{234}U have been determined. The elemental yields are shown in figures 4 and 5. The transition from symmetric fission in the lighter systems to asymmetric

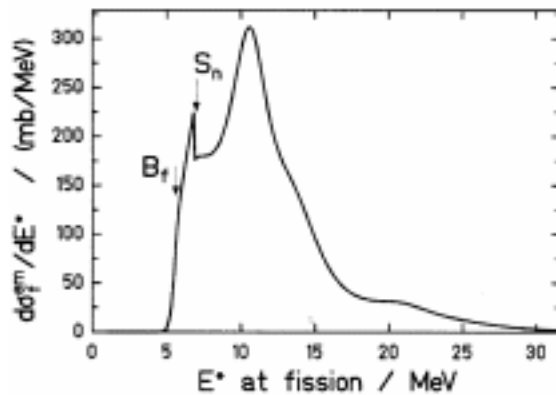


Figure 3. Calculated distribution of excitation-energies at fission after electromagnetic excitation of ^{234}U projectiles at 430 A MeV in a lead target.

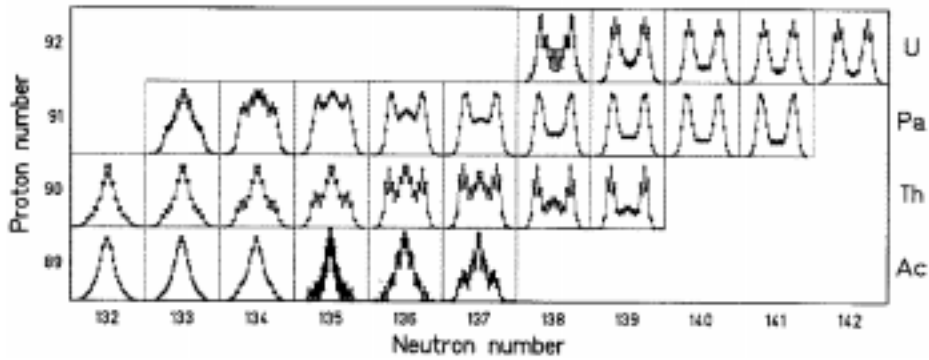


Figure 4. Measured fission-fragment charge distributions from ^{221}Ac to ^{234}U are shown on a chart of the nuclides.

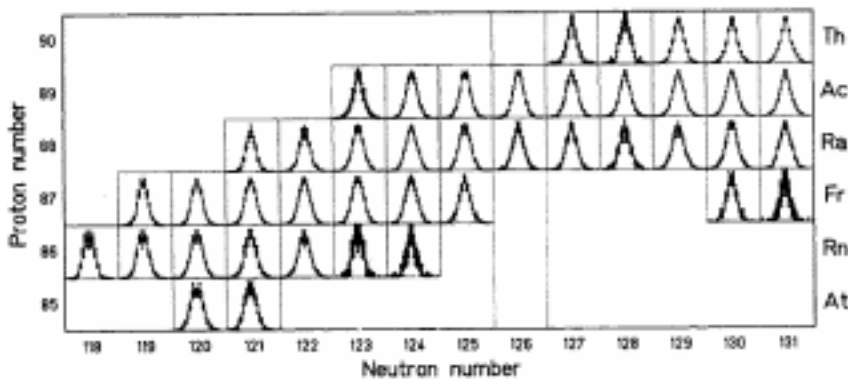


Figure 5. Measured fission-fragment charge distributions from ^{205}At to ^{221}Th are shown on a chart of the nuclides.

fission in the heavier systems is systematically covered. In the transitional region, around ^{226}Th , triple-humped distributions appear, revealing comparable intensities for symmetric and asymmetric fission. In particular, for uranium and thorium isotopes strong even-odd effects are observed.

4.1 Fission channels

Turkevich and Niday [7] already noticed that different components which they named as fission modes appear in the fission-fragment yields and in the kinetic-energy distributions. Later, models were proposed to deduce the fission characteristics from the properties of the scission configuration alone, e.g. ref. [8]. However, these neglect the dynamic evolution of the system from saddle to scission which seems to be very important [9–11]. The concept of independent fission channels has been developed [12,13] according to which

the fissioning system follows specific valleys in the potential energy in the direction of elongation. Several properties (e.g. average mass or charge split, mass or charge width, mean total kinetic energy) could be related to calculated properties of the highly deformed fissioning system. However, the mechanisms which determine the fission-fragment yields are not sufficiently well understood to allow for quantitative predictions. Therefore, the intensities of the fission channels are usually deduced from experiment.

The systematic survey on fissioning systems with strongly varying charge distributions (see figures 4 and 5) will provide a new test case for the concept of independent fission channels. Moreover, it will enable a more systematic view on how the intensities of the fission channels vary as a function of the nuclear composition. At first glance, two fission components appear in the measured charge distributions, a symmetric and an asymmetric one. The weights of these two fission components were quantitatively determined by fitting three Gaussian curves to the charge-yield distributions. The widths (standard deviation) of the symmetric and the asymmetric components were found to be close to 4.0 charge units and 2.2 charge units, respectively, for all nuclei for which they could be extracted. In cases where either one of the components was too weak, the corresponding value from this systematics was used. The ratio of symmetric to asymmetric fission was then determined by the ratio of the areas of the Gaussians describing the data. The result of this procedure is shown in figure 6. The transition is rather smooth and the weights of the two fission components scale with the mass of the fissioning nucleus.

The data on elemental yields support the idea, stated by Itkis *et al* [14,15], that the weights of the fission channels are principally determined by an interplay of the neutron shells at $N = 82$ and $N = 86$ with the liquid-drop potential. A quantitative description of this idea has been formulated by Benlliure *et al* [16] by relating the charge distributions to the density of transition states in the vicinity of the outer fission barrier. From the model calculations (figure 6) we can conclude that the transition from the asymmetric to the symmetric components is mainly determined by the variation in the stiffness of the liquid-drop potential.

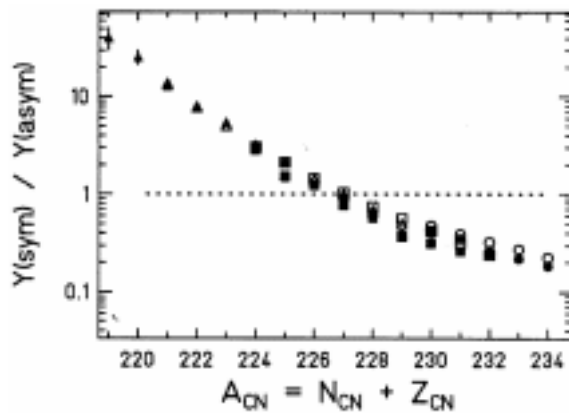


Figure 6. Intensity ratios of the symmetric and the asymmetric fission components in the transitional region as a function of mass number. The full triangles (squares, circles) correspond to thorium (protactinium, uranium) isotopes. The open symbols correspond to model calculations (see text).

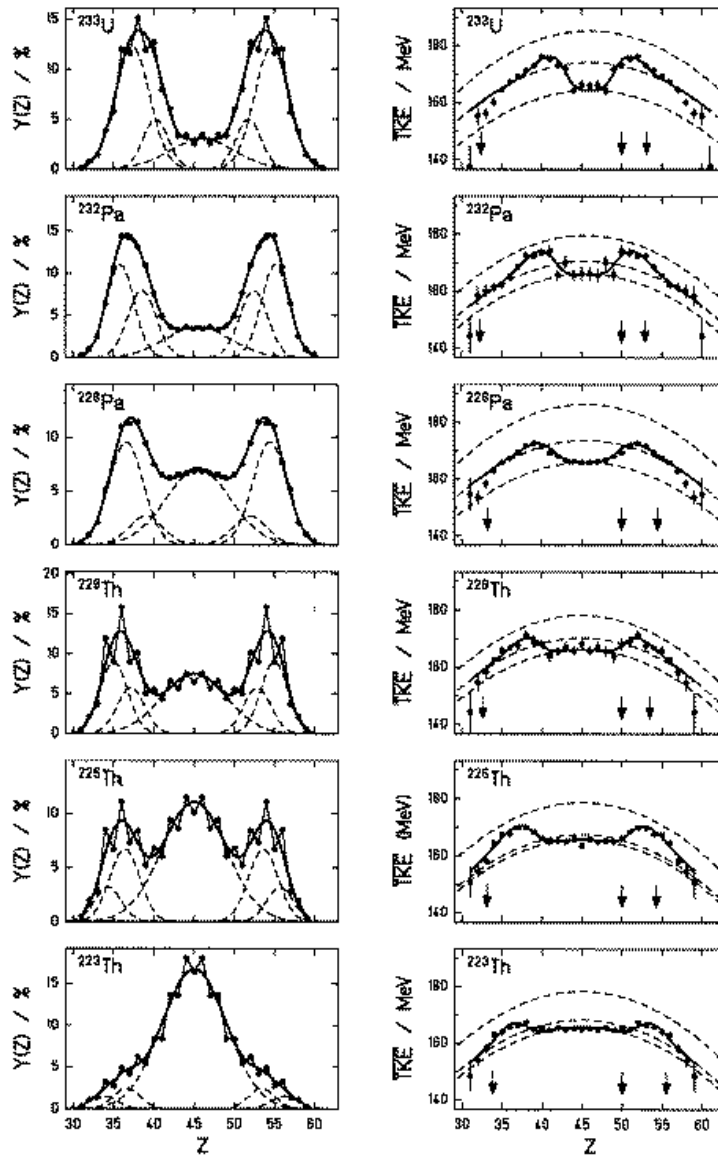


Figure 7. Measured elemental yields (left part) and average total kinetic energies (right part) as a function of the nuclear charge measured for fission fragments of several fissioning nuclei. Only statistical errors are given. The total kinetic energies are subject to an additional systematic uncertainty of 2%, common to all data [5]. Arrows indicate the positions of neutron ($N = 50, 82$) and proton shells ($Z = 50$). The positions of the neutron shells are calculated from the proton numbers by assuming an unchanged charge density (UCD). The full lines show descriptions with the model of independent fission channels. The contributions of the individual channels are depicted by dashed lines (see text for details).

4.2 Influence of shell structure

In detail, the charge-yield distributions and the total kinetic energies of ^{233}U , ^{232}Pa , ^{228}Pa , ^{228}Th , ^{226}Th , and ^{223}Th are shown in figure 7. The gross structural effects observed in the charge yields are different from those showing up in the total kinetic energies. From ^{233}U to ^{223}Th , the weight of the asymmetric fission component decreases strongly, while the enhancement of the total kinetic energies near $Z = 52$ to 54 is preserved. In a simultaneous fit to elemental yields and total kinetic energies, it was possible to reproduce these data with the assumption of independent fission channels. A description with two fission channels only, which well reproduces the nuclear-charge yields, represents the measured TKE values only poorly. A satisfactory description was obtained with three channels, ‘standard I’ at $N = 82$, ‘standard II’ around $N = 88$ in the heavy fragment, and ‘superlong’ at symmetry, using the notations introduced by Brosa *et al* [13]. Each channel was represented by a Gaussian distribution in the yields and a specific scission-point configuration. In order to consider the trivial variation of the total kinetic energy as a function of mass and charge split, the Coulomb repulsion V_C in the scission-point configuration was parametrized by the following expression, introduced in ref. [8]:

$$V_C = \frac{Z_1 \cdot Z_2 \cdot e^2}{r_0 \left(A_1^{1/3} \left[1 + \frac{2\beta_1}{3} \right] + A_2^{1/3} \left[1 + \frac{2\beta_2}{3} \right] \right) + d}. \quad (1)$$

Z_i , A_i and β are nuclear-charge numbers, mass numbers and deformations of the fission fragments respectively, $r_0 = 1.16$ fm is the nuclear-radius constant, and e the elementary charge. The mass numbers were related to the charge numbers by the UCD assumption. The deformation parameters were fixed at $\beta = 0.6$ as predicted by the liquid-drop model, see ref. [8]. The ‘tip distance’ d was determined from a fitting procedure, requiring that the measured TKE values are best reproduced by V_C . Since the fit can only yield one parameter of eq. (1), the elongation of the system, parametrized by the tip distance d , also effectively represents variations in the deformation of the fragments.

For each fission channel, position, width, and height of the Gaussian representing the nuclear-charge yields as well as the tip distance of the scission configuration were treated as free parameters. The width of the superlong channel had to be kept constant for the fit to converge. The yields are formulated as the sum and the total kinetic energies as the weighted average of the different components. Unfortunately, the dispersion of the total kinetic energy could not be deduced in the secondary beam experiment due to the limited resolution. Therefore, the relative weights of the two asymmetric fission channels could only be determined with rather large error bars.

As a remarkable result, we found that the superlong channel which appears at symmetry becomes more compact for the lighter systems as can be seen in figure 8. This finding indicates that this channel is influenced by shell effects, too, although the charge distribution can be represented by a simple Gaussian. The variation of the tip distance in the symmetric channel can be related to the properties of the shell around $N = 64$ which tends to become less deformed with decreasing neutron number (see e.g. refs [8,17]). Moreover, the symmetric channel appears to be much narrower than observed previously in heavier systems.

In figure 9 it is shown the evolution of the positions in charge and neutron number of both asymmetric fission channels (standard I and standard II) as a function of the mass

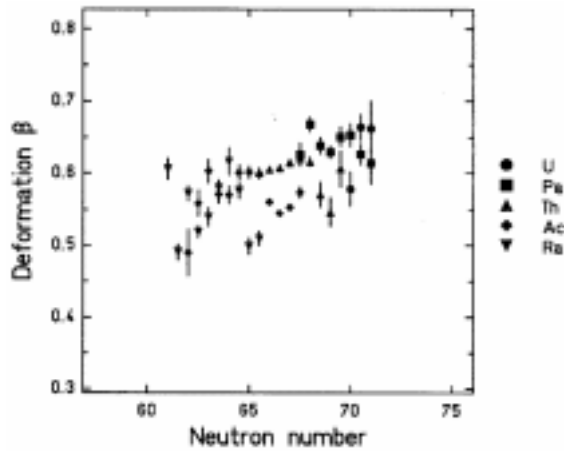


Figure 8. Evolution of deformation in the symmetric fission component obtained from the fits as a function of the neutron number of the fission fragments estimated assuming UCD.

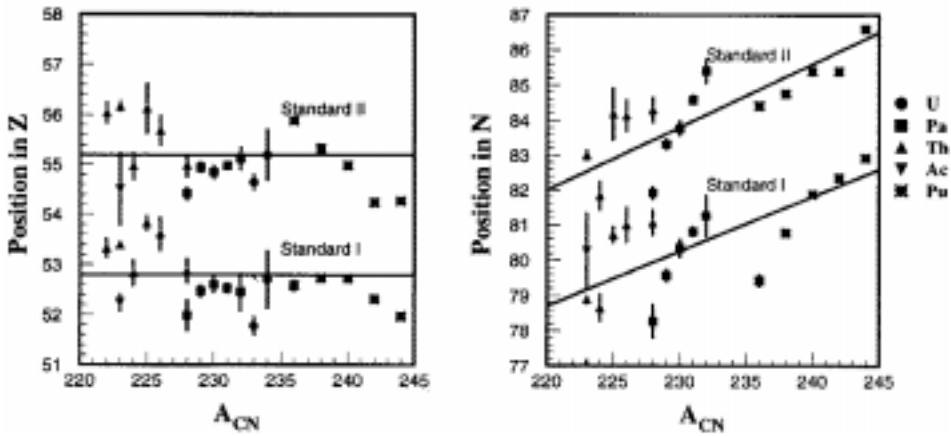


Figure 9. Position in nuclear charge and neutron number of the two asymmetric fission modes (standard I and standard II) as a function of the mass of the fissioning system. The data corresponding to the plutonium isotopes were taken from ref. [18]. The position in neutron number was estimated from the position in nuclear charge by the UCD assumption.

of the fissioning nucleus. We observe a constant position in charge corresponding to the values $Z = 53$ (standard I) and $Z = 55$ (standard II), while the positions in neutron number change with the mass of the fissioning nucleus. Since the two most important asymmetric fission channels (standard I and standard II) are usually associated [8] with the spherical $N = 82$ shell and the deformed $N = 88$ shell, respectively, this is a remarkable result.

From the good simultaneous description of nuclear-charge yields and total kinetic energies as demonstrated by figure 7 we conclude that the concept of independent fission channels has passed an important test although the parameters of the fission channels can not be directly related to the known properties of the nuclear shells. It allows for the strong variations of the yields while keeping the TKE distributions almost unchanged. However, we would also like to add a critical remark. In accordance with the usual treatment, the most probable scission-point configuration, parametrized by the tip distance d , was fixed at one value for each fission channel and not allowed to vary as a function of charge split. This might be a severe oversimplification. It is known that the energetically most favourable deformation in a deformed shell region varies with the number of nucleons [8,17]. Therefore a corresponding variation of the mean elongation at the scission point as a function of the charge split is to be expected. This would imply a variation of the most probable tip distance d even inside one fission channel. Besides the symmetric channel, this also concerns the standard II fission channel related to the $N = 88$ deformed shell. Therefore, part of the increase of the TKE values in the asymmetric component towards symmetry, which is attributed to the compact standard I channel in our description, may rather be imputed to a variation of the scission configuration in the standard II channel to more compact shapes. This would strongly affect all parameters of the two asymmetric fission channels.

5. Conclusion

A new experimental technique was applied to measure elemental yields and total kinetic energies after low-energy fission of short-lived radioactive nuclei. The beautiful data nicely demonstrate the decisive influence of nuclear structure on the fission process in a particular interesting transitional region around ^{227}Th . In contrast to the total kinetic energies, the element distributions were found to vary strongly, essentially as a function of mass number of the fissioning system. This behaviour could well be reproduced by the model of independent fission channels. The weights of the asymmetric fission channels decrease with decreasing mass of the fissioning nucleus, but the scission-point configurations remain unchanged. The scission-point configuration of the symmetric fission channel, however, evolves to more compact shapes for the lighter fissioning nuclei, where symmetric splits correspond to smaller nucleon numbers. This clearly reveals the influence of shell effects also in the symmetric channel. The analysis of both asymmetric channels (standard I and standard II) show that these two fission channels can not be explained by the influence of the shells $N = 82$ and $N = 88$.

References

- [1] H-G Clerc, M deJong, T Brohm, M Dornik, A Grewe, E Hanel t, A Heinz, A R Junghans, C Röhl, S Steinhäuser, B Voss, C Ziegler, K-H Schmidt, S Czajkowski, H Geissel, H Irnich, A Magel, G Münzenberg, F Nickel, A Piechacyek, C Scheidenberger, W Schwab, K Sümmerer, W Trinder, M Pfützner, B Blank, A Ignatyuk and G Kudyaev, *Nucl. Phys.* **A590**, 785 (1995)
- [2] A R Junghans, M de Jong, H-G Clerc, A V Ignatyuk, G A Kudyaev and K-H Schmidt, *Nucl. Phys.* **A629**, 635 (1998)
- [3] H Geissel, P Armbruster, K-H Behr, A Brünle, K Burkard, M Chen, H Folger, B Franczak, H Keller, O Klepper, B Langenbeck, F Nickel, F Pfeng, M Pfützner, E Roeckl, K Rykaczewski,

- I Schall, D Schardt, C Scheidenberger, K-H Schmidt, A Schröter, T Schwab, K Sümmerer, M Weber, G Münzenberg, T Brohm, H-G Clerc, M Fauerbach, J-J Gaimard, A Grewe, E Hanelt, B Knödler, M Steiner, B Voss, J Weckenmann, C Ziegler, A Magel, H Wollnik, J P Dufour, Y Fujita, D J Vieira and B Sherrill, *Nucl. Instrum. Methods* **B70**, 286 (1992)
- [4] A Grewe, S Andriamonje, C Böckstiegel, T Brohm, H-G Clerc, S Czajkowski, E Hanelt, A Heinz, M G Itkis, M de Jong, M S Pravikoff, K-H Schmidt, W Schwab, S Steinhäuser, K Sümmerer and B Voss, *Nucl. Phys.* **A614**, 400 (1997)
- [5] C Böckstiegel, S Steinhäuser, J Benlliure, H-G Clerc, A Grewe, A Heinz, M de Jong, A R Jung-hans, J Müller and K-H Schmidt, *Phys. Lett.* **B398**, 259 (1997)
- [6] B Baur and C A Bertulani, *Phys. Rev.* **C34**, 1654 (1986)
- [7] A Turkevich and J B Niday, *Phys. Rev.* **84**, 52 (1951)
- [8] B D Wilkins, E P Steinberg and R R Chasman, *Phys. Rev.* **C14**, 1832 (1976)
- [9] P Möller and S G Nilsson, *Phys. Lett.* **B31**, 283 (1970)
- [10] G A Kudyaev, Yu B Ostapenko and G N Smirenkin, *Sov. J. Nucl. Phys.* **45**, 951 (1987)
- [11] H Kudo, H Muramatsu, H Nakahara, K Miyano and I Kohno, *Phys. Rev.* **C25**, 3011 (1982)
- [12] V V Pashkevich, *Nucl. Phys.* **A169**, 275 (1971)
- [13] U Brosa, S Grossmann and A Müller, *Phys. Rep.* **197**, 167 (1990)
- [14] M G Itkis, Yu Ts Oganessian, G Chubarian, V N Okolovich and G N Smirenkin, in *Nuclear Fission and Fission-Product Spectroscopy* edited by H Faust and G Fioni (ILL Grenoble, 1994) pp. 77
- [15] M G Itkis, V N Okolovich, A Yu Rusanov and G N Smirenkin, *Sov. J. Part. Nucl.* **19**, 301 (1988)
- [16] J Benlliure, A Grewe, M de Jong, K-H Schmidt and S Zhdanov, *Nucl. Phys.* **A628**, 458 (1998)
- [17] I Ragnarsson and R K Sheline, *Phys. Scr.* **29**, 385 (1984)
- [18] L Dematté, C Wagemans, R Barthélémy, P D'hondt and A Deruytter, *Nucl. Phys.* **A617**, 331 (1997)